TRANSPLANT INTERNATIONAL

Transplant International ISSN 0934-0874

ORIGINAL ARTICLE

Ultra-short echo-time magnetic resonance imaging distinguishes ischemia/reperfusion injury from acute rejection in a mouse lung transplantation model

Natalie C. Chuck,[1] Andreas Boss,[1] Moritz C. Wurnig,[1] Markus Weiger,[2] Yoshito Yamada[3] and Wolfgang Jungraithmayr[3]

1 Institute for Diagnostic and Interventional Radiology, University Hospital Zurich, Zurich, Switzerland
2 Institute for Biomedical Engineering, University of Zurich and Swiss Federal Institute for Technology, Zurich, Switzerland
3 Division of Thoracic Surgery, University Hospital Zurich, Zurich, Switzerland

Keywords
lung transplantation, mouse, magnetic resonance imaging, ultra-short echo-time.

Correspondence
Natalie C. Chuck, MD, Institute for Diagnostic and Interventional Radiology, University Hospital Zurich, Rämistrasse 100, 8091 Zurich, Switzerland.
Tel.: +41 44 255 11 11;
fax: +41 44 244 44 43;
e-mail: nataliechuck@gmail.com

Conflict of interest
There is no conflict of interest for any of the authors.

Received: 3 March 2015
Revision requested: 7 April 2015
Accepted: 28 August 2015
Published online: 7 October 2015

doi:10.1111/tri.12680

Summary

To investigate whether lung tissue characterization by ultra-short echo-time (UTE) magnetic resonance imaging (MRI) allows ischemia/reperfusion injury to be distinguished from acute rejection in a mouse lung transplantation model. After orthotopic lung transplantation with 6 mice receiving syngeneic (C57Bl/6) lung transplants and 6 mice receiving allogeneic (BALB/c) transplants, they underwent postoperative imaging using three-dimensional UTE-MRI (echo times TE = 50–5000 μs) and conventional T2-weighted fast spin-echo imaging. Quantitative T2* values of lung transplant parenchyma and spin density (SD) were compared by region-of-interest analysis. All samples underwent histological and immunohistochemical workup. In the allogeneic group, alveolar infiltration resulting from acute organ rejection was visualized in the UTE sequences. This was reflected by the quantitative measurements of SD and T2* values with higher values in the allogeneic group compared with the syngeneic group and nontransplanted lung at the first time point (24 h postoperative: Tx allogeneic group SD: 2133.9 ± 516; Tx syngeneic group SD: 1648.61 ± 271; $P = 0.004$; Tx allogeneic group T2*: 1710.16 ± 644 μs, Tx syngeneic group T2*: 577.16 ± 263 μs; $P = <0.001$). Changes caused by acute rejection after lung transplantation can be visualized and characterized using a UTE sequence due to different relaxation properties compared with both syngeneic lung transplants and normal lung tissue.

Introduction

Lung transplantation has become an established therapeutic option for patients with end-stage lung disease [1]. Ischemia/reperfusion (I/R) injury and acute rejection (AR) are common complications after lung transplantation and can threaten the graft [2–4]. Both are known to be a risk factor for the development of chronic rejection or bronchiolitis obliterans syndrome (BOS) [5]. Beyond the first year of transplantation, BOS (or chronic rejection) accounts for over 25% of deaths [6]. Additionally, the incidence of chronic rejection approaches 50% within 5 years of transplantation [6,7] and the median survival after the diagnosis of chronic rejection is only 3 years [8].

Acute rejection has been identified as a strong risk factor for chronic rejection [9,10]. Different complications, for example, acute rejection, primary graft disease, or chronic rejection and infections, have to be identified early as they are treated differently [11]. Early detection and differential diagnoses of acute I/R injury versus AR may allow for appropriate treatment reducing transplant failure and the risk for subsequent development of chronic rejection.

In clinical routine, computed tomography is a common tool for assessing lung pathologies [12], but due to low

specificity of current imaging methods, histological workup of lung tissue, especially after lung transplantation, is mandatory. This requires an invasive procedure, for example, transbronchial biopsies (TBB) that come with certain risks, for example, bleeding (and aspiration of blood) and pneumothorax. MR imaging could help assessing who is in need of a TBB and who could be spared the procedure [13–16].

Magnetic resonance imaging allows for noninvasive functional assessment and *in vivo* visualization of the anatomy with high spatial resolution without using ionizing radiation. MRI of the lung is still challenging due to low proton density and short T2* transverse relaxation time of the inflated lung [17,18]. The short T2* time is caused by the unique architecture of the lung with air/soft tissue interfaces of the alveoli creating microscopic inhomogeneities of the static magnetic field with a broad intravoxel Larmor frequency distribution. The fast signal decay precludes depiction of lung parenchyma using conventional MRI sequences with Cartesian k-space acquisition schemes with a lower limit of the achievable echo-time TE in the order of 1–2 ms.

Previous studies have shown that using ultra-short echo-time (UTE) MRI in conjunction with acquisition of the free inducting decay (FID) allows for a reduction of TE to less than 100 μs. Slice-selective pulse sequences with TEs in the range of 5-200 μs can be produced by the use of half radiofrequency (rf) excitations with radial sampling from the center of the k-space [19]. Even shorter excitation pulses and thus shorter TE are enabled by nonselective three-dimensional (3D) UTE imaging [20]. Signal decay from spin excitation until the echo can therefore be drastically reduced, and thus, a higher signal-to-noise ratio (SNR) can be achieved compared with conventional image sequences with short TE [21–24].

In previous studies, we showed that MR imaging of the lung using UTE can help identify I/R injury in the lung parenchyma after lung transplantation and provides additional information compared with high-resolution micro-computed tomography [25,26]. In this study, we investigate whether lung tissue characterization by computation of spin density (SD) and apparent T2* relaxation times obtained from UTE sequences allows I/R injury to be distinguished from acute allograft rejection after unilateral mouse lung transplantation.

Materials and methods

Animals

The experimental protocol was approved by the institutional animal committee (license number 02/2010). Twelve laboratory animals (inbred mice) from the strain C57Bl/6 (H-2K^b), weighing 25–30 gr, were used as transplant recipients. Six animals (inbred mice) from the strain BALB/c (H-2K^d) served as donors for the allografts. Six C57Bl/6 mice served as donors for the syngrafts. Animals received adequate strict care according to The Principles of Laboratory Animal Care (promulgated in 1985 and most recently revised in 1996). No special preparation of the animals for the experiment was applied except the adapting and housing conditions.

Orthotopic single lung transplantation

Orthotopic lung transplantation was adapted from the technique described by Jungraithmayr *et al* [27]. Donor mice were anesthetized with a mixture of medetomidine (1 mg/kg) and ketamine (75 mg/kg) intraperitoneally. After tracheostomy, the mouse was connected to a ventilator (UNO microventilator UMV-03, UNO Roestvaststaal, Zevenaar, the Netherlands). Abdomen and thorax were opened, and the lungs were flushed with 5 ml Perfadex® (Vitrolife, Göteborg, Sweden) through the arteria pulmonalis. The heart–lung block was excised and put on ice. Explanted donor lungs were exposed to 8 h of cold ischemia time in both groups. For the transplant recipient procedure, the hilum of the left lung was dissected and artery, vein, and bronchus were cuffed. Afterward, the recipient was anesthetized with isoflurane (Isoba®, Schering-Plough, Uxbridge, UK) in an induction box. The animal was intubated and connected to the ventilator with a mixture of 50% O_2, 50% room air, and 2.5% isoflurane. After thoracotomy, artery, vein, and bronchus were separated from each other and 10-0 ligatures were placed around the structures. Microvascular clamps were put on artery and vein. First, the vein was anastomosed, then the artery, and subsequently the bronchus. The clamps were released (first vein, then artery) and the lung inflated. The chest was then closed and the animal allowed to wake up. Pain medication, with buprenorphine (0.1 mg/kg every 8 h during 3 days, Temgesic®, Schering-Plough) was given as soon as the animals regained full consciousness.

Histology, H&E, and Immunohistochemistry for CD3

On day 1, 3, and 7, transplanted lungs were excised, and the middle third of the pulmonary graft was recovered for histological evaluation.

After fixation in 4% phosphate-buffered formalin, the lungs were cut transversally into 2-mm-thick slices and embedded in paraffin. Four-micrometer-thick sections were cut and mounted on positively charged glass slides. Standard histological procedures (hematoxylin and eosin (H&E) and immunostaining for CD3) were performed using the CD3 antibody (rat antimouse, BD Pharmingen, Franklin Lakes, NJ, USA).

Magnetic resonance imaging

Imaging was performed in a Bruker 4.7T PharmaScan 47/40 with a gradient strength of 375 mT/m and a slew rate of 3375 T/m/s, equipped with a linearly polarized bird-cage 1H mouse whole-body RF coil. The animal bed was equipped with a pad with continuous warm water supply to prevent the mouse from cooling.

During image acquisition, the mice were anesthetized with 0.6% isoflurane (1-Chlor-2,2,2-trifluorethyl-difluoromethylether; Attane; Minrad I, Buffalo, NY, USA) mixed with 100% oxygen. The animal's eyes were protected from drying by applying sterile ophthalmic ointment (Vit. A Crème, Bausch & Lomb Swiss AG, Steinhausen, Switzerland).

After gradient-echo (GRE) localizers in 3 spatial directions, the imaging protocol included a 2D-encoded T2w fast spin-echo (FSE) sequence (TR/TE: 2500 ms/11 ms; effective TE: 33 ms; echo train length: 8; matrix: 256 × 256; field of view (FoV): 40 × 40 mm; slice thickness: 1 mm; averages: 3). For relaxation measurement, a 3D UTE sequence was applied with 8 subsequent acquisitions with TE = 50, 75, 100, 500, 1500, 3000, 4000, and 5000 μs, respectively. Further protocol parameters of the UTE sequence were as follows: repetition time (TR) = 8 ms, matrix = 128 × 128 × 128, FoV = 45 × 45 × 45 mm, spatial resolution = 0.35 × 0.35 × 0.35 mm, flip angle = 5°, averages = 1, and acquisition time = 6 m 50s. The *k*-space trajectory associated with the gradient ramps was measured *in vivo* once for each physical gradient axis and employed proportionally to each gradient direction.

Data analysis

We evaluated six different regions of interest (RoI) positions per mouse: the normal and the transplanted lung in the basal part, peripherally on the level of the hilum and the apical part (typical RoI positioning is shown in Fig. S1). RoIs were placed manually to avoid overlap with bronchi/pleural effusion and pneumothoraces. In the respective RoIs, spin density S_0 and apparent transverse relaxation T2* times were calculated by pixelwise mono-exponential fitting via scripts written in Matlab (The Mathworks, Natick, MA, USA). Signal intensities were previously corrected for different receiver gain values using the calibrated receiver gain function and for the automatic mapping of the data to the image gray value scale. The fitting routine used a nonlinear least-squares fit of the measured signal intensities to the expression

$$S(\mathrm{t}) = S_0 \times e^{-\mathrm{t}/\mathrm{T2}*} + N$$

via an algorithm based on the interior-reflective Newton method. Fitting variables were S_0, which is a value proportional to spin density, and the T2* time constant. The noise term N was not fitted but estimated as the standard deviation (SD) in a RoI selected in the image background outside the object avoiding regions masked due to the radial acquisition. For statistical analysis, mean values and standard deviations were computed. The two-sided paired Student's t-test was used to test for significance of T2* values and spin density S_0 between RoIs of the transplanted and the normal lung. *P*-values <0.05 were considered statistically significant. All statistical analyses were performed using commercially available software (SPSS, release 17.0, Chicago, IL USA).

Results

Histology and CD3 immunohistochemistry

H&E staining of specimen sections were performed at three different time points after Tx according to the MRI measurements: 1, 3, and 7 days following lung transplantation. At day one, syngeneic transplants showed diffuse flooding by innate immune cells such as macrophages and neutrophils into the lung parenchyma (Fig. 1a) and thickening of the alveolar wall due to edema. Three days after transplantation, there were still considerable amounts of graft-infiltrating cells, but reduced when compared to day 1 (Fig. 1b). At day 7, cell infiltration has largely resolved and alveolar architecture was visible, revealing only scattered innate immune cells within the alveolar wall. Also, edema has cleared nearly completely (Fig. 1c). By contrast, AR after allogeneic transplantation induces unique histological features which profoundly differ from the histological pattern observed in I/R injury. Here, cells of the adaptive immune system, mainly T and B cells, do not infiltrate the transplant diffusely but they accumulate specifically around vessels, and later also around bronchi. This can be observed 1 day after transplantation (Fig. 1d). These cuffs of cells increase in size over time (Fig. 1e) and are at a maximum at day 7 when AR inflammation is thought to be full blown (Fig. 1f).

When comparing allogeneically transplanted lungs at day 3 after transplantation (Fig. 2a) with their contra-lateral, naïve lungs, we could observe a considerable influx of leukocytes (Fig. 2b). In contrast to the transplanted lung, these cells infiltrated the pulmonary parenchyma in a diffuse manner. Immunohistochemistry for CD3 of respective sections identified those infiltrating cells as $CD3^+$ T cells (Fig. 2c and d).

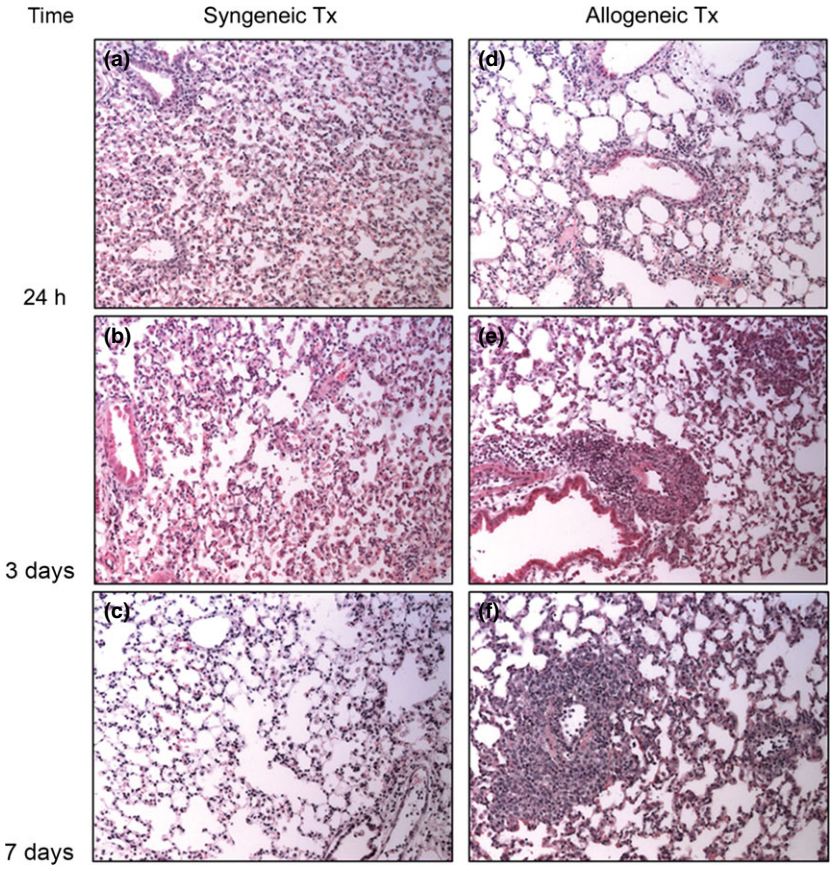

Figure 1 Representative images (H&E) of the course after mouse lung transplantation in syngeneic lung transplants at 1 day (a), 3 days (b), and 7 days (c) after transplantation, and in allogeneic lung transplant at respective time points (d–f). (Magnification, ×200; data are representative of six experiments).

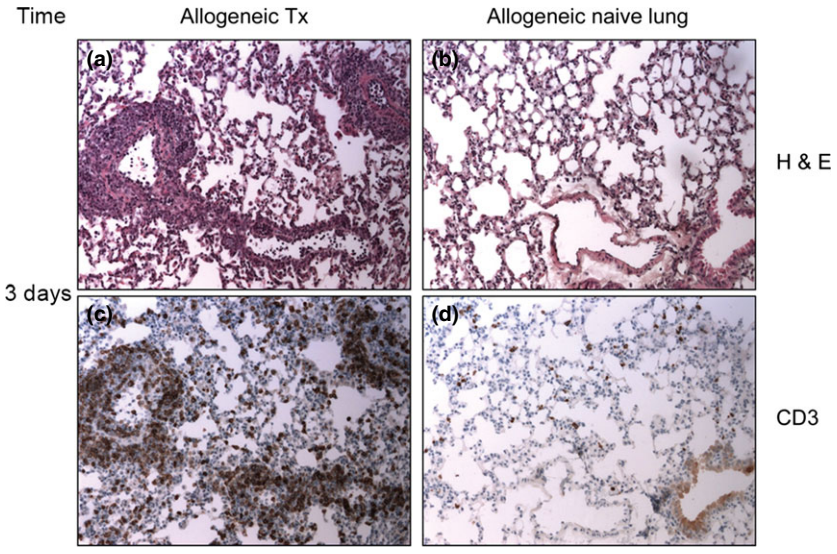

Figure 2 Representative images (H&E) of an allogeneic mouse lung transplant 3 days after transplantation (a) and the corresponding section from the contralateral, naïve lung (b). Immunohistochemistry for CD3 reveals $CD3^+$ T cells at day 3 after lung transplantation (c) and in the corresponding section from the contralateral, naïve lung (d). (Magnification, ×200; data are representative of six experiments.)

Conventional Imaging using T1w and T2w sequences

The T2w sequence showed good image quality, both being hampered in phase direction by pulsation artifacts of the heart and smearing artifacts caused by breathing (Fig. 3a and e). On the first time point, the lung parenchyma showed no detectable signal for either the normal or the transplanted lung in both sequences. T2w allowed for detection of the small pleural effusions that were visible in all animals of both groups. In the syngeneic group, pleural effusions were completely resolved by the second and third time points, while in the allograft group, 5 of 6 mice showed residual small pleural effusions on the third time point. Pneumothoraces could not be identified in both sequences due to the lack of signal.

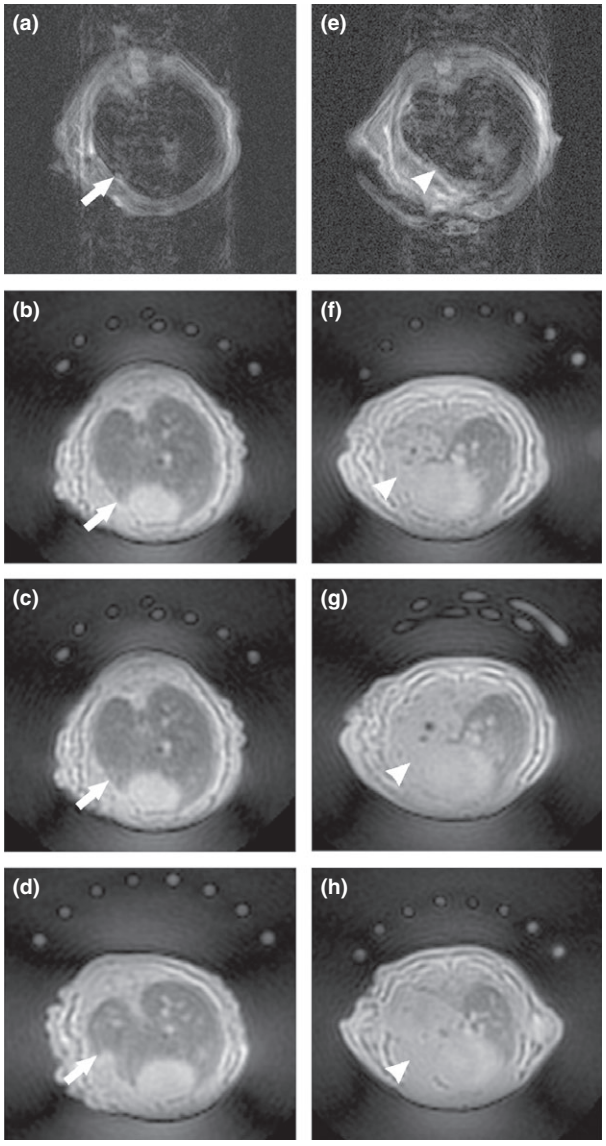

Figure 3 Typical images of a syngeneic lung transplant in the left row (images a-d) and of an allogeneic lung transplant (images e–h). a/e: Fast spin-echo images (TE = 11 ms, syngeneic and allogeneic transplanted lung marked with an arrow and an arrowhead, respectively) demonstrating complete signal loss of lung parenchyma. b-d, f-h: Ultra-short echo-time images (TE = 50 μs) at different slice position. The syngeneic transplanted lung on the left side (marked with an arrow) exhibits nearly the same signal as the naive lung on the right side. Lung tissue and interstitial structures are well visualized. The allogeneic transplanted lung (marked with an arrowhead) appears distinctly hyperintense when compared to the naïve lung. On image g, the segmental bronchi can be appreciated.

Qualitative findings using the UTE sequence

The UTE sequence exhibited good image quality, and especially the sequences with low echo times proved robust against smearing and pulsation artifacts caused by heart beat and breathing. The sequence acquired with 50 μs showed no pulsation artifacts at all. Artifacts increased with longer TE (Fig. 4).

In all UTE acquisitions, a discrete Gibb's ringing artifact was noticeable at the interface between the thoracic wall and the lung parenchyma slightly affecting the image quality of the lungs. Small pneumothoraces were clearly identifiable in the UTE sequences in the left hemithorax on the first time point, and on the second and third time points, these were resolved.

In the syngraft group, there was no visually noticeable difference of signal intensity between the lung transplant and the nontransplanted lung concerning the parenchyma (Fig. 5b–d). In the allograft group, all six mice showed distinct pattern of alveolar infiltration, discriminating an air bronchogram; the alveolar infiltration increased in the subsequent images on the second and third time points (see quantitative evaluation below; Fig. 5f–h). Just like in the syngraft group, the pneumothoraces were resolved at the later time points.

Quantitative spin density and T2* relaxation measurements

Spin density and T2* measurements for the syngeneic and allogeneic group are depicted in Table 1. Typical T2* decay curves are shown in Fig. 5.

Syngrafts—spin density

Twenty-four hours after transplantation, SD (mean = 1648 ± 271, n = 18: 6 mice and 3 RoI analyses each) was significantly higher in the transplanted compared with the normal lung (1319 ± 379, n = 18) ($P < 0.0001$). The measured values 168 h after transplantation (1562 ± 329, n = 18) assimilated to the values of the normal lung parenchyma (1359 ± 408, n = 18), but with a statistically significant difference remaining ($P < 0.001$).

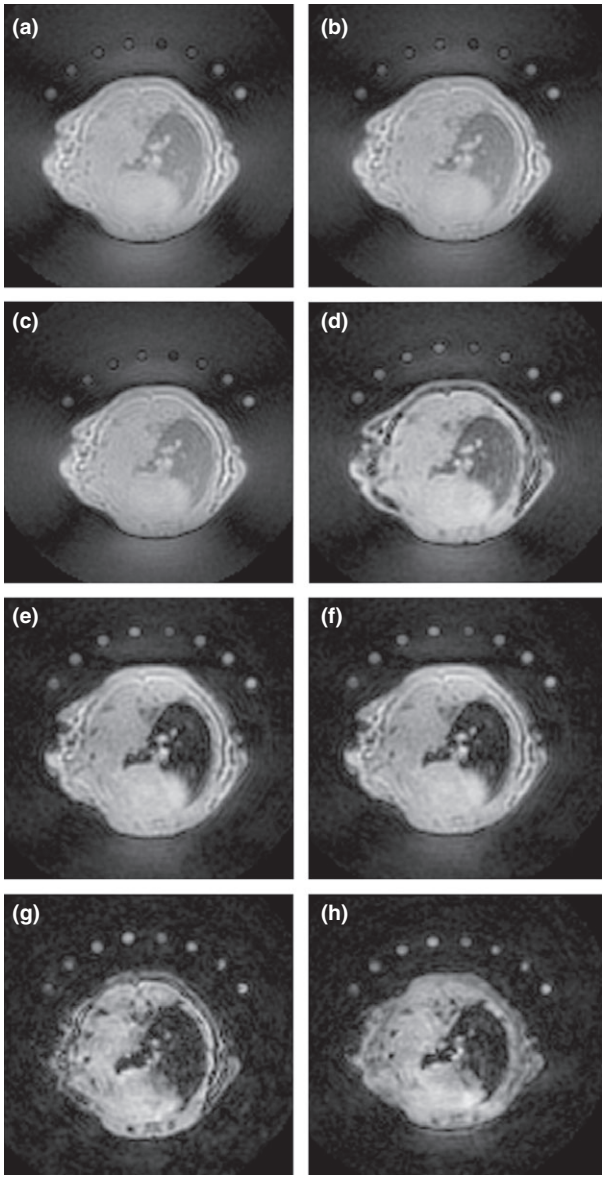

Figure 4 Representative ultra-short echo-time images of an allogeneic lung transplant illustrating the T2* signal decay in the healthy lung parenchyma in the right hemi thorax with increasing echo-time TE. The ultra-rapid decay of transverse magnetization of lung tissue is caused by microscopic magnetic field inhomogeneities between tissue and air interfaces of the alveoli. a: TE 50 μs, b: 75 μs, c: 100 μs, d: 500 μs, e: 1500 μs f: 3000 μs; g: 4000 μs; h: 5000 μs.

Syngrafts—T2 relaxation time*

There was no significant difference ($P = 0.19$) between the transplanted lung (577 ± 263 μs, $n = 18$) and the normal lung (515 ± 180 μs, $n = 18$) 24 h after transplantation. Seventy-two hours after transplantation, 461 ± 159 μs was measured in the transplanted lung versus 572 ± 162 μs in the naïve lung, which proved to be statistically significant ($P < 0.05$). Hundred and sixty-eight hours after transplantation, no significant difference ($P = 0.62$) between the transplanted (501 ± 211 μs, $n = 18$) and the naïve (480 ± 183 μs, $n = 18$) lung was observed.

Allografts—spin density

Twenty-four hours after transplantation, the transplanted lung showed higher spin density (2133 ± 516, $n = 18$, $P < 0.01$) compared with the nontransplanted lung (1286 ± 390, $n = 18$), which persisted after 72 h ($P < 0.0001$) with measurements for the transplanted lung being 2005 ± 252, $n = 18$ and for the nontransplanted lung 1525 ± 298, $n = 18$. The difference remained significant ($P < 0.0001$) at the last time point (168 h), with a spin density of 2097 ± 324, $n = 18$ for the transplanted lung and 1418 ± 303, $n = 18$ for the nontransplanted lung.

Allografts—T2 relaxation time*

A significant difference ($P < 0.0001$) was found 24 h after transplantation when comparing the transplanted (1558 ± 797 μs, $n = 18$) with the nontransplanted lung (526 ± 223 μs, $n = 18$). Seventy-two hours after transplantation, the difference for the relaxation times remained significant ($P < 0.000001$) with measurements of 1710 ± 644 μs, $n = 18$ for the transplanted lung and 653 ± 186 μs, $n = 18$ for the nontransplanted lung. The same was true ($P < 0.01$) for the last measurement, 168 h after transplantation, where values of 1659 ± 1246 μs, $n = 18$ for the transplanted lung and 573 ± 191 μs, $n = 18$ for the nontransplanted lung were measured.

Syn- versus Allografts

When comparing the transplanted lung of the syngraft against the allograft group, significant differences for spin density measurements were observed at all time points (24 h: $P < 0.0001$; 72 h: $P < 0.000000001$; 168 h: $P < 0.01$). The same was true for measurements of T2* relaxation time (24 h: $P < 0.0001$; 72 h: $P < 0.00001$; 168 h: $P < 0.001$). When comparing the nontransplanted lung of both groups, a higher spin density was measured at all the three time points in the allograft group compared with the syngraft group (24 h: $P < 0.01$; 72 h: $P < 0.0001$; 168 h: $P < 0.0001$). For T2* relaxation time measurements of the nontransplanted lung, no statistically significant difference was measurable, regardless of the time following the operation (24 h: $P = 0.9$; 72 h: $P = 0.24$, 168 h: $P = 0.08$; Fig. 6).

Discussion

In this study, we showed that applying UTE sequences could be helpful in distinguishing ischemia/reperfusion injury from acute rejection after lung transplantation.

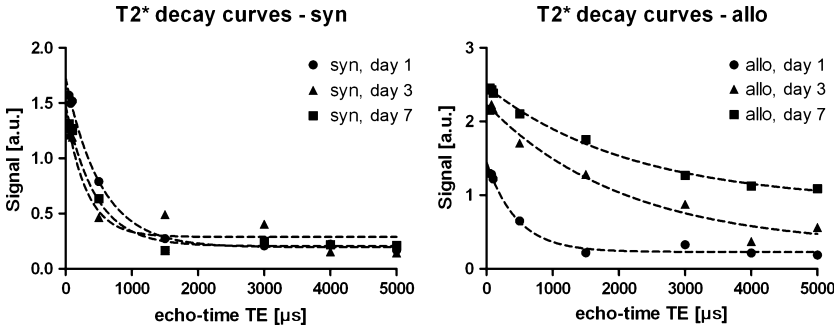

Figure 5 Typical T2* decay curves of the apparent transverse magnetization for transplanted lungs at different time points are shown. A good approximation of the fitting curves (straight lines) to the measurements points can be seen. Whereas in syngeneic lung transplants (left side), only slightly increased spin density (intercept with *y*-axis) can be noted for the first examination time point with subsequent normalization, a progressive deterioration is seen in the allogeneic lung transplants with increasing spin density (pulmonary infiltration) and slower decay of magnetization (loss of ventilation).

Table 1. Quantitative measurements of spin density (SD) and T2* relaxation time—Comparison between the transplanted and the naïve lung in the (a) syngeneic group, (b) allogeneic group.

	Naive lung		Tx lung		*P* value	
Time after Tx (h)	Spin density (a.u.)	T2* relaxation time (ms)	Spin density (a.u.)	T2* relaxation time (ms)	SD	T2*
Syngrafts						
24	1319 ± 379	515 ± 180	1648 ± 271	577 ± 263	$P < 0.05$	n.s.
72	1406 ± 247	572 ± 162	1561 ± 284	461 ± 159	$P < 0.05$	$P < 0.05$
168	1359 ± 408	480 ± 163	1562 ± 329	501 ± 211	$P < 0.05$	n.s.
Allografts						
24	1386 ± 390	526 ± 223	2133 ± 516	1558 ± 797	$P < 0.05$	$P < 0.05$
72	1525 ± 298	653 ± 186	2005 ± 252	1710 ± 644	$P < 0.05$	$P < 0.05$
168	1418 ± 303	573 ± 191	2097 ± 324	1659 ± 1246	$P < 0.05$	$P < 0.05$

Using tissue characterization techniques with computation of T2* relaxation times and spin densities, a different behavior could be identified for both I/R injury (represented by the syngraft group) and AR (represented by the allograft group). In the I/R group (syngrafts), alterations of the biomarkers (spin density and T2* relaxation time) were detected early after the transplantation but not as strong as in the AR group (allografts; 30% higher for SD in the allograft group compared with the syngraft group, 170% higher for T2* for the allograft group compared with the syngraft group); compared with the AR group, these alterations vanished in the following time points representing the diminishing I/R.

Moreover, typical complications seen after lung transplantation such as pneumothoraces or pleural effusion could easily be detected with a combination of conventional and ultra-short echo-time sequences: Pneumothoraces were only visualized in the ultra-short echo-time sequences due to their capability to detect signal in the inflated lung, whereas pleural effusion was better visualized in T2-weighted conventional sequences. Moreover, we were able to show that the deterioration of the normal lung in the allogeneic graft subjects was detectable in the spin density measurements using UTE sequences.

Two phenomena can occur during the early course after lung transplantation: I/R injury and AR. In spite of the introduction of improved preservation solutions, I/R injury is an inevitable event which hampers the early postoperative course of lung transplantation. As a consequence, the pulmonary endothelium is severely injured by reactive oxygen species allowing for the influx of fluid with subsequent development of alveolar edema. I/R injury is additionally aggravated by an influx of cells of the innate immune system such as activated macrophages and neutrophils which diffusely infiltrate the lung parenchyma. In contrast to I/R injury, AR is a response of the adaptive immune system toward the foreign engrafted organ. Here, in sharp contrast to I/R injury, clusters of lymphocytes typically accumulate around vessels and airways in order to exert their inflammatory activity. Another feature of AR versus I/R injury is that the development of edema is less pronounced. Complicating the clinical picture, both condition an overlap with

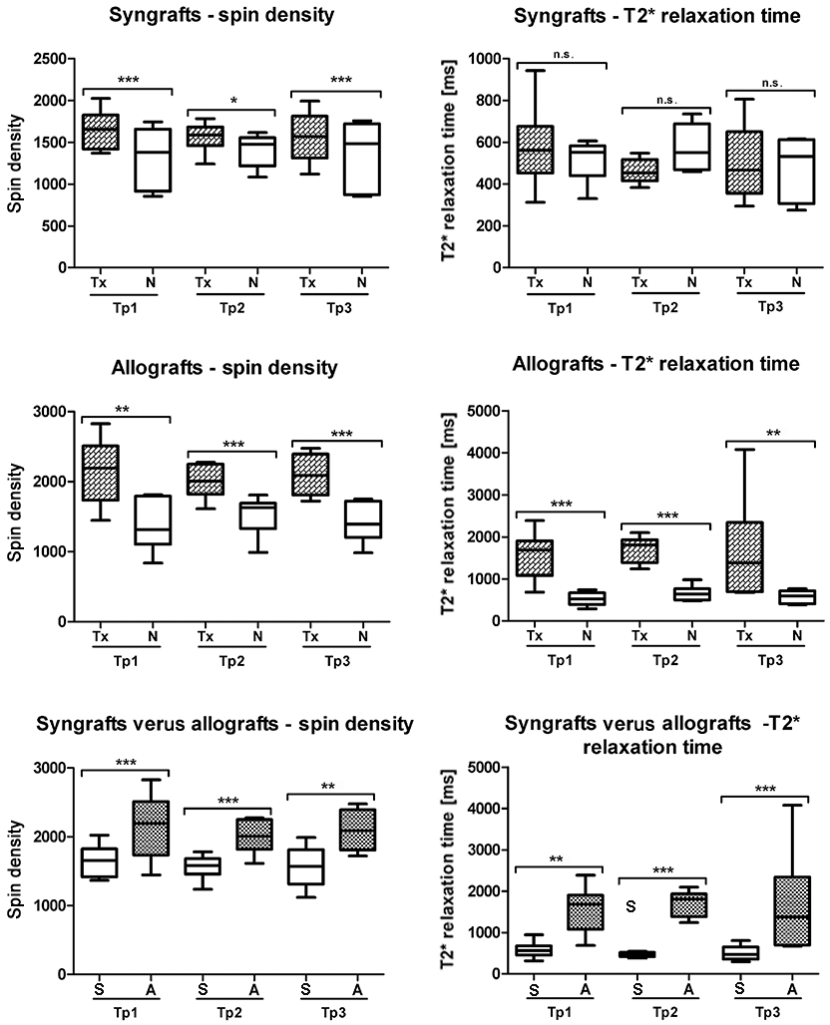

Figure 6 Box-and-whisker plots comparing the spin density and T2* relaxation times for the syngraft group (upper row) on the three different time points and the allograft group (middle row), respectively. In the lowest row: box-and-whisker plots comparing spin density and T2* relaxation time of the syngraft group versus the allograft group at all the three time points. Note: *$P < 0.05$, **$P < 0.01$, ***$P < 0.001$, Tx: lung transplant, N: naïve lung, Tp1: 24 h after unilateral lung transplantation, Tp2: 72 h after unilateral lung transplantation, Tp3: 168 h after unilateral lung transplantation.

respect to time. They can even occur simultaneously, which makes the clinical scenario most difficult to distinguish one event from the other. Usually, once the I/R injury is resolved (usually within 2 or 3 days), AR becomes visible. AR almost never occurs before day 2 or 3 post-Tx at the earliest as AR is triggered by the adaptive immune system, meaning that T cells, which are the key immune cells for the development of AR, need to be activated and proliferate during this time period of 2 or 3 days.

Thus, day 3 post-Tx is kind of an overlapping time point from resolving of I/R injury and onset of AR in which the one from the other cannot be 100% differentiated. However, in this allogeneic model with prolonged ischemia, I/R injury is always resolving while AR from day 3 is ongoing.

As the mode of treatment differs between I/R injury and AR considerably, it is of major importance to be able to distinguish precisely between these two pathologic entities. The methodological application presented here seems to be an initial approach in differentiating between these two distinct events.

Computed tomography (CT) is the gold standard for displaying lung parenchymal pathologies, and it is widely applied in humans to diagnose unspecific pathologies which can arise following lung transplantation, such as bacterial or viral pneumonia, or lymphomas. However, specific pathology patterns directly associated with the transplantation procedure, namely I/R injury and AR, are scarcely defined/described in human imaging modalities. Yet, there are attempts to describe pathologic patterns of post-

transplant injuries using CT, even though the descriptions are rather unspecific: I/R injury is described as air space consolidation and AR patterns as ground-glass opacities and interlobular septal densities [28,29]. None of these findings could be associated with the histopathological proof of AR at transbronchial biopsy [30].

HR-CT is commonly used in clinical routine for the detection of lung pathologies after lung transplantation; however, HR-CT suffers from its low specificity regarding the imaging findings. Distinguishing the origin of the imaging findings remains challenging. This is the main reason for investigating new MRI techniques, which may provide a better characterization of tissue changes after transplantation. Reports on the application of MRI depicting post-transplant-related injuries are essentially lacking in humans. There is one experimental study using MRI in a model of heterotopic lung transplantation in which ultrasmall superparamagnetic iron oxide particles are used to detect acute lung allograft rejection [31]. However, iron oxide particles were incorporated only by macrophages, and not by lymphocytes, the cell type that is considered the most important during AR.

A phenomenon that is frequently described after lung transplantation is the involvement of cell infiltration by recipient-derived circulating cells into the contralateral, nontransplanted lung. While this event was found after I/R injury in a canine model of lung transplantation in the nonischemic contralateral lung [32], in our study the group of allo-transplantation showed a considerably higher frequency of cells within the contralateral lung. This finding should draw attention to the fact that remote effects from both I/R injury and AR can affect distant organs.

When comparing the transplanted with the naïve lung, the allograft group showed higher values for both, spin density and T2*.

On the other side, when looking at the transplanted versus the naïve lung in the syngraft group, higher values were only found for spin density, whereas T2* remained the same for the transplanted and the naïve lung. We interpreted this as an expression of persistent good ventilation of the lung parenchyma of the transplanted lung resulting in short T2* due to microscopic tissue–air interfaces in spite of the influx of cells leading to a higher spin density value in the transplanted lung.

As shown before [26], the use of UTE sequences with echo times below 1 ms allows for visualization of the lung parenchyma. Applying a protocol with different echo times in the UTE sequences permitted a pixel-on-pixel calculation of the decay time T2* of transverse magnetization, and therefore, a quantification of what was well visualized on the images acquired. Corresponding to the previous studies, the visualization of postoperative pneumothoraces was only possible in the UTE sequences with a very low echo time, but for a complete overview over the pulmonary state, conventional T2 fast spin-echo sequences were necessary to identify pleural effusion.

Our study shows some limitations. First, we did not use a device for respiratory triggering. Due to the fast repetition time, applying respiratory triggering is not straightforward. Conventional respiratory triggering with one excitation per respiratory cycle results in a strong increase in the acquisition time of the very short TE sequence. In mice, there is no relevant degradation of image quality due to respiratory motion. However, in human studies, the issue of respiratory motion will probably become important. Second, the very low soft tissue contrast can be seen as a disadvantage when compared to conventional sequences. Combining conventional, especially T2-weighted, sequences with UTE sequences currently seems to provide the most information regarding postoperative changes such as pleural effusion, pneumothoraces, and atelectasis. Third, we did not address the problem of infections which is a major early complication after lung transplantation. In the mouse model, this is hardly ever relevant as mice almost never suffer from post-transplant infectious diseases such as pneumonia. In patients, however, it could be difficult to distinguish infection from acute rejection, even more as similar laboratory parameters are altered. Similarly, in HR-CT, it is difficult to distinguish infection from acute rejection (ground-glass opacities, lung consolidation). It remains to be shown whether relevant differences may be detected in UTE-MRI, for example due to differences in ventilation resulting in different T2* properties.

Fourth, in clinical transplantation, I/R occurs within the first 36 hours, whereas acute rejection, with the use of potent immunosuppressants, usually does not occur until weeks or months later. In a clinical setting, the discrimination between chronic allograft rejection versus infection and other pathologies will be more important. This study was designed to get a better understanding of the changes of MR biomarkers after lung transplantation. In a step-by-step approach, we try to reach the ultimate goal of a reliable distinction between chronic rejection from other sources of signal alterations. The induction of chronic rejection in a mouse model proves to be much more challenging when compared to the induction of acute rejection, and only recently, we have been able to see significant signs of chronic rejection in histological samples of our mouse models.

The animal model of lung transplantation and the imaging protocol presented might serve as another step toward the development of a treatment algorithm focusing on the alleviation of I/R injury after transplantation or suppression of acute transplant rejection. This model relies on MR imaging features that can help to distinguish between these pathological entities. Due to the completely noninvasive

nature of the MRI examination, this experimental model is well suited for longitudinal. The translation of the proposed imaging protocol to a study in human subjects seems straightforward as UTE, and the closely related zero echotime (ZTE) sequences [33] for clinical MR imagers have become commercially available. In clinical imaging, medical devices can present a contraindication for MR imaging, for example cardiac pacemakers. Nowadays, most surgical clips, pulmonary artery catheters, etc. are MR compatible and physiology monitoring and ventilation are possible in MR examinations. In our institution, many critically ill patients undergo MR examinations, but of course one has to take into account that examination time and patient preparation are more extensive than in CT [R2 C5].

We conclude that small animal MRI using a combination of conventional and UTE sequences is suitable for investigating acute pathologies following lung transplantation. Relaxation measurements computing T2* times and spin densities allow distinguishing between the two most common early complications after lung transplantation, I/R injury and acute rejection.

Authorship

NCC: involved in data acquisition (imaging), evaluated the data and wrote the manuscript. AB: provided idea/concept and statistics, evaluated the data and wrote the manuscript. MCW: involved in data evaluation and statistics. MW: wrote the manuscript. Yoshito Yamada: involved in data acquisition (operation, histology). WJ: provided idea/concept, involved in data acquisition (operation, histology), evaluated the data and wrote the manuscript.

Funding

No funding was received concerning this study.

Supporting Information

Additional Supporting Information may be found in the online version of this article:

Figure S1. Exemplary images (UTE sequence TR 8 ms/TE 50 μs) of the typical RoI positioning are shown.

References

1. Theodore J, Lewiston N. Lung transplantation comes of age. *N Engl J Med* 1990; **322**: 772.
2. King-Biggs MB. Acute pulmonary allograft rejection. Mechanisms, diagnosis, and management. *Clin Chest Med* 1997; **18**: 301.
3. Trulock EP. Lung transplantation. *Am J Respir Crit Care Med* 1997; **155**: 789.
4. Frist WH, Loyd JE, Merrill WH, *et al.* Single lung transplantation: a temporal look at rejection, infection, and survival. *Am Surg* 1994; **60**: 94.
5. Bando K, Paradis IL, Similo S, *et al.* Obliterative bronchiolitis after lung and heart-lung transplantation. An analysis of risk factors and management. *J Thorac Cardiovasc Surg* 1995;**110**:4; discussion -4.
6. Christie JD, Edwards LB, Aurora P, *et al.* Registry of the International Society for Heart and Lung Transplantation: twenty-fifth official adult lung and heart/lung transplantation report–2008. *J Heart Lung Transplant* 2008; **27**: 957.
7. Meyers BF, de la Morena M, Sweet SC, *et al.* Primary graft dysfunction and other selected complications of lung transplantation: a single-center experience of 983 patients. *J Thorac Cardiovasc Surg* 2005; **129**: 1421.
8. Valentine VG, Robbins RC, Berry GJ, *et al.* Actuarial survival of heart-lung and bilateral sequential lung transplant recipients with obliterative bronchiolitis. *J Heart Lung Transplant* 1996; **15**: 371.
9. Hachem RR, Khalifah AP, Chakinala MM, *et al.* The significance of a single episode of minimal acute rejection after lung transplantation. *Transplantation* 2005; **80**: 1406.
10. Hopkins PM, Aboyoun CL, Chhajed PN, *et al.* Association of minimal rejection in lung transplant recipients with obliterative bronchiolitis. *Am J Respir Crit Care Med* 2004; **170**: 1022.
11. Paradis IL, Duncan SR, Dauber JH, Yousem S, Hardesty R, Griffith B. Distinguishing between infection, rejection, and the adult respiratory distress syndrome after human lung transplantation. *J Heart Lung Transplant* 1992; **11**(4 Pt 2): S232.
12. Hansell DM. High-resolution computed tomography in the evaluation of fibrosing alveolitis. *Clin Chest Med* 1999; **20**: 739, viii.
13. Brenner DJ, Hall EJ. Computed tomography–an increasing source of radiation exposure. *N Engl J Med* 2007; **357**: 2277.
14. Maher MM, Kalra MK, Toth TL, Wittram C, Saini S, Shepard J. Application of rational practice and technical advances for optimizing radiation dose for chest CT. *J Thorac Imaging* 2004; **19**: 16.
15. Willekens I, Buls N, Lahoutte T, *et al.* Evaluation of the radiation dose in micro-CT with optimization of the scan protocol. *Contrast Media Mol Imaging* 2010; **5**: 201.
16. Brouwers JE, van Rietbergen B, Huiskes R. No effects of in vivo micro-CT radiation on structural parameters and bone marrow cells in proximal tibia of wistar rats detected after eight weekly scans. *J Orthop Res* 2007; **25**: 1325.
17. Bergin CJ, Noll DC, Pauly JM, Glover GH, Macovski A. MR imaging of lung parenchyma: a solution to susceptibility. *Radiology* 1992; **183**: 673.
18. Gamsu G, Sostman D. Magnetic resonance imaging of the thorax. *Am Rev Respir Dis* 1989; **139**: 254.
19. Robson MD, Gatehouse PD, Bydder M, Bydder GM. Magnetic resonance: an introduction to ultrashort TE (UTE) imaging. *J Comput Assist Tomogr* 2003; **27**: 825.

20. Glover GH, Pauly JM, Bradshaw KM. Boron-11 imaging with a three-dimensional reconstruction method. *J Magn Reson Imaging* 1992; **2**: 47.
21. Gewalt SL, Glover GH, Hedlund LW, Cofer GP, MacFall JR, Johnson GA. MR microscopy of the rat lung using projection reconstruction. *Magn Reson Med* 1993; **29**: 99.
22. Bergin CJ, Pauly JM, Macovski A. Lung parenchyma: projection reconstruction MR imaging. *Radiology* 1991; **179**: 777.
23. Kuethe DO, Adolphi NL, Fukushima E. Short data-acquisition times improve projection images of lung tissue. *Magn Reson Med* 2007; **57**: 1058.
24. Olsson LE, Lindahl M, Onnervik PO, *et al.* Measurement of MR signal and T2* in lung to characterize a tight skin mouse model of emphysema using single-point imaging. *J Magn Reson Imaging* 2007; **25**: 488.
25. Wurnig MC, Tsushima Y, Weiger M, Jungraithmayr W, Boss A. Assessing lung transplantation ischemia-reperfusion injury by microcomputed tomography and ultrashort echo-time magnetic resonance imaging in a mouse model. *Invest Radiol* 2014; **49**: 23.
26. Jungraithmayr W, Chuck N, Frauenfelder T, Weder W, Boss A. MR imaging by using very short echo-time sequences after syngeneic lung transplantation in mice. *Radiology* 2012; **265**: 753.
27. Jungraithmayr WM, Korom S, Hillinger S, Weder W. A mouse model of orthotopic, single-lung transplantation. *J Thorac Cardiovasc Surg* 2009; **137**: 486.
28. Krishnam MS, Suh RD, Tomasian A, *et al.* Postoperative complications of lung transplantation: radiologic findings along a time continuum. *Radiographics* 2007; **27**: 957.
29. Ng YL, Paul N, Patsios D, *et al.* Imaging of lung transplantation: review. *AJR Am J Roentgenol* 2009;**192** (3 Suppl):S1, quiz S4-9.
30. Gotway MB, Dawn SK, Sellami D, *et al.* Acute rejection following lung transplantation: limitations in accuracy of thin-section CT for diagnosis. *Radiology* 2001; **221**: 207.
31. Kanno S, Lee PC, Dodd SJ, Williams M, Griffith BP, Ho C. A novel approach with magnetic resonance imaging used for the detection of lung allograft rejection. *J Thorac Cardiovasc Surg* 2000; **120**: 923.
32. Palazzo R, Hamvas A, Shuman T, Kaiser L, Cooper J, Schuster DP. Injury in nonischemic lung after unilateral pulmonary ischemia with reperfusion. *J Appl Physiol* (1985) 1992; **72**: 612.
33. Weiger M, Pruessmann KP. *MRI with Zero Echo Time*. Hoboken: *eMagRes*, 2012; **1**: 311-322.